Journal of Molecular Structure 1304 (2024) 137666

Contents lists available at ScienceDirect

Journal of Molecular Structure

journal homepage: www.elsevier.com/locate/molstr

Characterization of the synthesized diaqua-bis(indazole-κN^2)bis(nitrato-κO)zinc(II) complex and DFT calculations

Ceyhun Kucuk [a,*], Sibel Celik [b], Senay Yurdakul [c], Namık Özdemir [d], Hakan Bülbül [e]

[a] Ahmet Erdogan Vocational School of Health Services, Zonguldak Bulent Ecevit University, Zonguldak, Turkey
[b] Vocational School of Health Services, Kırsehir Ahi Evran University, 40100 Kırşehir, Turkey
[c] Department of Physics, Faculty of Science, Gazi University, Ankara
[d] Department of Mathematics and Science Education, Faculty of Education, Ondokuz Mayıs University, 55139 Samsun, Turkey
[e] Department of Physics, Faculty of Science, Ondokuz Mayıs University, 55139 Samsun, Turkey

ARTICLE INFO

Keywords:
Indazole
zinc nitrate
DFT
XRD
AIM

ABSTRACT

In this study, the diaqua-bis(indazole-κN^2)bis(nitrato-κO)zinc(II) complex has been examined by using single-crystal X-ray diffraction (XRD) and spectroscopic analysis methods (FT-IR, UV-Vis). The Zn(II) ion is hexa-coordinated, and the coordination environment around Zn(II) is best considered as a slightly distorted octahedral geometry. The theoretical calculations were carried out using the density functional theory (DFT) method. Hydrogen bonding in particular has been assessed through topological analysis using methods like electron localization function (ELF), localized orbital locator (LOL), natural bond orbital analysis (NBO), and the atoms in molecules method (AIM). Also, the reduced density gradient approach (RDG) has been used to determine the strong and weak attractive, repulsive, and van der Waals interactions in the title complex. The Hirsfeld surface analysis was used to investigate the nature of the crystal structure's intermolecular interactions. The reactivity of the complex was investigated through the use of MEP and HOMO-LUMO studies. The molar conductivity values of the compounds provided evidence of their non-electrolytic nature, while thermal data indicated that the complexes decompose into metal oxide residue in five stages.

1. Introduction

Indazole is a bicyclic, heterocyclic, and organic molecule consisting of a pyrazole ring fused with a benzene ring. It belongs to the azole family and contains carbon, hydrogen, and nitrogen atoms in its structure [1]. This molecule has three tautomeric structures: 1H-indazole, 2H-indazole, and 3H-indazole. However, the most widely used tautomeric form is 1H-indazole [2]. The majority of drugs used in the treatment of diseases are heterocyclic molecules containing N atoms in their structure [3]. Indazole molecule is used as a basic scaffold in pharmaceutical products [4] due to its many biological activities, such as antimicrobial, antifungal, antiviral, anticancer, anti-inflammatory, anticancer, and anti-HIV [5].

Zinc is probably appealing for application in chemistry catalysis due to its low toxicity, low cost, abundance, and ease of distribution [6]. Also, Zn(II) is the second most abundant trace element in the human body after iron and is essential in many biological systems [7].

The formation of complexes in coordination with the O- and N-terminals of biologically active organic compounds of transition metals provides advantages in drug production by changing the coordination number, geometry, and redox states [8]. In addition, metal complexes have structural instability and are very sensitive to the molecular environment. This allows them to react easily [9]. In the literature, there are many transition metal complexes synthesized from indazole and its derivatives. In a study, the silver nitrate complex of the indazole molecule was synthesized, and characterization and DFT calculations were carried out. Additionally, the antioxidant and antimicrobial activities of the synthesized structure were evaluated [10]. In another study, the silver (I) complex salt of the Bis(4,5-dihydro-1H-benzo[g]indazole) molecule that is an indazole derivative was synthesized, and structural characterization and DFT calculations were performed [11]. Zn, Ni, Co, Fe, and Mn metal complexes of the indazole-3-carboxylic acid molecule were also synthesized in another study. Also, DFT calculations, molecular docking, and molecular dynamics simulations were performed for the obtained structures [12].

In many studies conducted today, different molecular modeling tools

* Corresponding author.
E-mail address: ceyhun.kucuk@beun.edu.tr (C. Kucuk).

https://doi.org/10.1016/j.molstruc.2024.137666
Received 25 November 2023; Received in revised form 26 January 2024; Accepted 27 January 2024
Available online 31 January 2024

or computer simulations are used to explain or verify the physical and chemical properties of a structure. Ab initio methods are calculation methods that can be performed without knowing any experimental data about the system [13]. DFT calculations, performed without the need for any experimental data, are one of the calculation methods that allow us to theoretically obtain the structural and spectroscopic properties of organic or inorganic molecules obtained by experimental methods in the most accurate way [14].

In this study, the diaqua-bis(indazole-κN^2)bis(nitrato-κO)zinc(II) complex was synthesized and its single crystal structure was obtained. The characterization of the synthesized complex was performed by X-ray crystallography and IR spectroscopy. DFT calculations for the title complex were carried out and compared with the experimental spectroscopic data. In addition, the electronic and thermodynamic properties of the synthesized complex were explained by the theoretical calculation method.

2. Material and Methods

2.1. Computational method

Geometric optimization, frequency, electronic, and thermodynamic properties were calculated using a combination of B3LYP functional and 6-311++G(d,p) (for C, H, N, and O) and SDD (for Zn) basis sets in density functional theory [15] with the Gaussian 09 package program [16,17]. UV-Vis calculations were carried out at the TD-DFT/B3LYP/SDD levels of theory in DMSO solvent using the IEFPCM model [18]. Images of the optimized geometric structure, frontier molecular orbital, and molecular electrostatic potential (MEP) maps were created with the Gauss View 5.0 program [19]. Electron localization function (ELF), localized orbital locator (LOL) surface maps, and dual descriptor images were created with the Multiwfn program [20]. Topological investigations of base pairs at various orientations were performed using the Multiwfn [21] and molecular visualization VMD [22] software programs. Analysis of the non-covalent interaction index (NCI) also permits a thorough examination of the interactions between two monomeric units within a complex. The NBO calculations were carried out with the NBO program embedded in Gaussian 09 software [23].

2.2. Experimental methods

2.2.1. Synthesis method

Indazole and zinc nitrate were obtained from Sigma-Aldrich Chemical Company and were used without any purification. In the synthesis step, firstly, 2 mmol solutions of indazole in 20 ml of ethanol and 1 mmol Zn(NO3)2 · 6H2O solutions in 10 ml of ethanol were prepared and stirred at 50°C for about 15 minutes. Then the prepared $Zn(NO3)_2$ $6H_2O$ solution was added dropwise to the indazole solution and stirred at 50°C for 2 hours. The resulting mixture was kept at +4°C for 3 months, and white crystal structures were obtained. The chemical formula of the resulting complex is $Zn(C_7H_6N_2)_2(NO_3)_2(H_2O)_2$. The Differential Scanning Calorimetry Thermogravimetry Analysis (TGA) was performed in a dynamic N_2 atmosphere (40 ml/min) with a heating rate of 25°C/min from a surrounding temperature of 1400°C/min using a Mettler Toledo thermal analyzer.

2.2.2. Spectral analyses

Far-IR and FT-IR spectra were recored in the regions of 500-100 cm^{-1} and 4000-500 cm^{-1} with the Bruker Vertex 80 FT-IR (the optical system enables to collect data over a total range of 900 to 5 cm^{-1} with resolution of 0.06 cm^{-1}, DTGS detector) and PerkinElmer Froniter Optica spectrometers (the optical system enables to collect data over a total range of 7800 to 350 cm^{-1} (1.28 to 28 xm) with resolution of 0.4 cm^{-1}, $LiTaO_3$ detector), respectively. The Uv-Vis spectrum was recorded between 190 and 1100 nm using an Agilent HP 8453 spectrophotometer. With the Mettler Toledo thermal analyzer, differential scanning calorimetry and thermogravimetry analysis (DSC/TGA) were performed in a dynamic N2 atmosphere (40 mL/min) with a heating rate of 25°C/min from the 1400°C/min ambient temperature.

2.2.3. X-ray crystallography

X-ray diffraction data of the synthesized Zn(II) complex were collected on a STOE IPDS II diffractometer at room temperature using graphite-monochromated Mo Kα radiation by applying the ω-scan method. Data collection and cell refinement were carried out using X-AREA [24], while data reduction was applied using X-RED32 [24]. The structure was solved by a dual-space algorithm using SHELXT-2018 [25] and refined by means of the full-matrix least-squares calculations on F^2 using SHELXL-2019 [26]. The coordinates of the H atoms of the water molecule were determined by a difference Fourier map and refined isotropically. All remaining H atoms were located in difference maps and then treated as riding atoms, fixing the bond lengths at 0.86 and 0.93 Å for NH and CH atoms, respectively. The displacement parameters of the H atoms were constrained as $U_{iso}(H) = 1.2U_{eq}$ of the parent atom. The indazole ring of the complex, except for the coordinated nitrogen atom at the 2-position, was disordered over two positions, and the refined site-occupancy factors of the disordered atoms are 0.593(4)% for the major position and 0.407(4)% for the minor position, respectively. Crystal data, data collection, and structure refinement details are collected in Table 1. Molecular graphics were created using OLEX2 [27].

3. Results and Discussion

3.1. Description of the structure

The solid-state structure of the synthesized Zn(II) complex has been unambiguously determined by single-crystal X-ray diffraction analysis, and its structural plot is presented in Fig. 1.

The asymmetric unit of the diaqua-bis(indazole-κN^2)bis(nitrato-κO) zinc(II) comprises an indazole ligand with a Zn(II) metal center as well as one nitrate anion and a water solvent molecule that coordinate to the metal atom. The Zn^{II} ion occupies an inversion center with the symmetry

Table 1
Crystal data and structure refinement parameters for the diaqua-bis(indazole-κN^2)bis(nitrato-κO)zinc(II).

CCDC depository	2286961
Color/shape	Colorless/prism
Chemical formula	$[Zn(NO_3)_2(C_7H_6N_2)_2(OH_2)_2]$
Formula weight	461.70
Temperature (K)	296(2)
Wavelength (Å)	0.71073 Mo Kα
Crystal system	Monoclinic
Space group	$P2_1/c$ (No. 14)
Unit cell parameters	
a, b, c (Å)	10.2679(11), 7.4896(5), 13.0226(14)
α, β, γ (°)	90, 107.910(8), 90
Volume (Å^3)	952.94(16)
Z	2
$D_{calc.}$ (g/cm^3)	1.609
μ (mm^{-1})	1.345
Absorption correction	None
F_{000}	472
Crystal size (mm^3)	0.54 × 0.55 × 0.46
Diffractometer	STOE IPDS II
Measurement method	ω scan
Index ranges	$-13 \le h \le 13$, $-8 \le k \le 9$, $-16 \le l \le 16$
θ range for data collection (°)	$2.084 \le \theta \le 27.413$
Reflections collected	14988
Independent/observed reflections	2168/1745
Refinement method	Full-matrix least-squares on F^2
Data/restraints/parameters	2168/356/215
Goodness-of-fit on F^2	1.047
Final R indices [$I > 2\sigma(I)$]	$R_1 = 0.0333$, $wR_2 = 0.0835$
R indices (all data)	$R_1 = 0.0472$, $wR_2 = 0.0891$
$\Delta\rho_{max.}$, $\Delta\rho_{min.}$ (e/Å^3)	0.30, −0.28

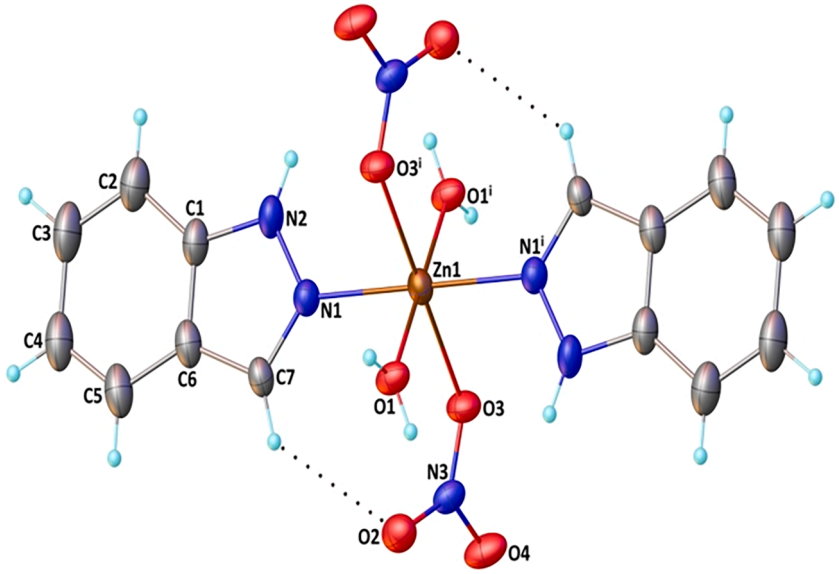

Fig. 1. Molecular structure of the diaqua-bis(indazole-κN^2)bis(nitrato-κO)zinc(II) showing atom-numbering scheme. Displacement ellipsoids are drawn at the 30% probability level and only the major part of the disordered atoms is shown for clarity

code (i) = $-x$, $-y+1$, $-z+1$. Hence, the ligands in the complex molecule are symmetry-related. The metal center exhibits a N_2O_4 coordination environment that is established by two nitrogen atoms from two indazole rings, two oxygen atoms from two nitrate ligands, and two oxygen atoms from two water molecules. Although the *trans* angles in the coordination sphere are all exactly 180° because of symmetry requirements, the *cis* bond angles change from 83.95(7) to 96.05(7)°, indicating that the octahedral coordination geometry around the metal atom is distorted.

The Zn—$N_{indazole}$ bond length is shorter than those found in bis (hydrotris(indazol-1-yl)borato)-zinc(II) dioxane solvate (1/3.5) [2.157 (3), 2.156(3) and 2.149(3) Å] [28] and that found in diaqua-bis (2-(indazol-1-yl)-2-thiazoline-N,N')-zinc(II) dinitrate [2.185(2) Å] [29], but slightly longer than that found in catena-[(4,4′-bipyridine)-bis (μ-indazole-5-carboxylato)-di-zinc N,N-dimethylformamide solvate] [1.987(4) Å] and catena-[(μ-3,6-di(pyridin-4-yl)-1,2,4,5-tetrazine)-bis (μ-1H-indazole-5-carboxylato)-di-zinc unknown solvate] [2.000(5) Å] [30]. The Zn—$O_{nitrate}$ bond distance is longer than those found in [1-(1-Naphthyl)-N,N-bis(pyridin-2-ylmethyl)methanamine]-(nitrato-O, O')-(nitrato-O)-zinc(II) [2.079(1) and 2.114(1) Å] [31], those found in

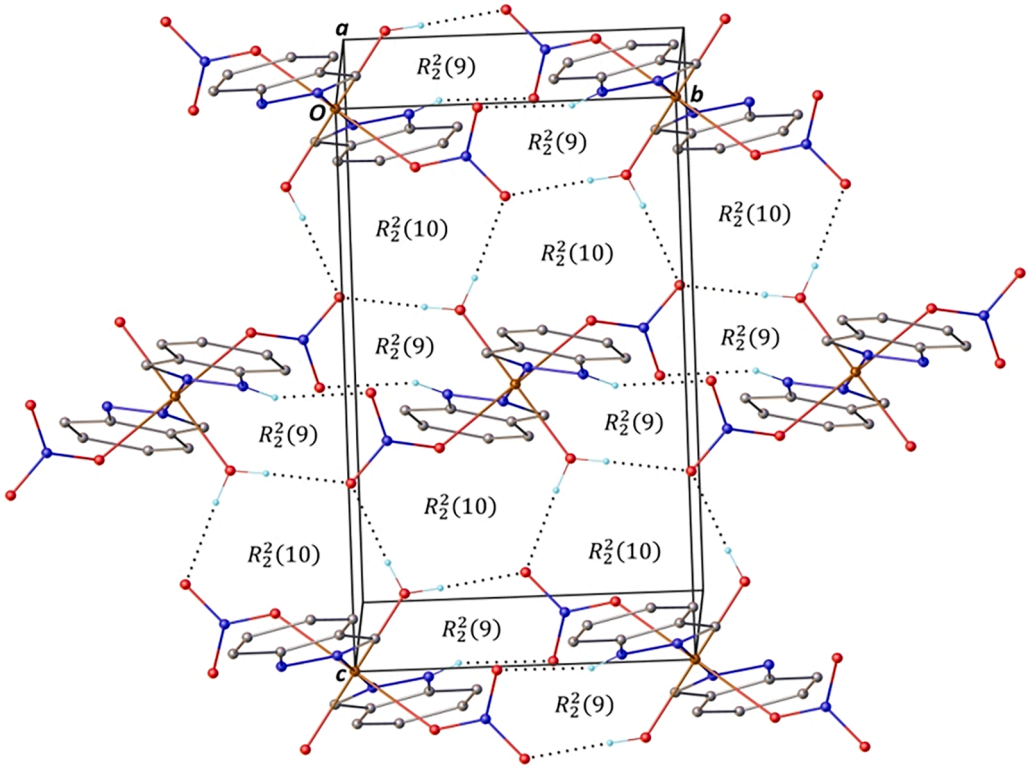

Fig. 2. Part of the crystal structure of the diaqua-bis(indazole-κN^2)bis(nitrato-κO)zinc(II), showing the formation of $R_2^2(10)$ and $R_2^2(9)$ rings. For the sake of clarity, H atoms not involved in the motifs shown have been omitted.

4,7,13,16,21,24-hexaoxa-1,10-diazoniabicyclo[8.8.8]-hexacosane tetra (nitrato)zinc(II) [1.999(2), 1.987(2), 2.010(2) and 2.008(2) Å] [32] and those found in bis(imidazole-κN^3)bis(nitrato-κO)zinc(II) [1.966 (3) and 1.999 (3) Å] [33]. The Zn—O_{water} bond length is similar to those observed in aqua-bis(1,5-dimethyl-2-phenyl-4-(((*E*)-4-pyridylmethylene)amino)pyrazolidin-3-one-κ*N*)-(nitrato-κ*O*)-(nitrato-$\kappa^2 O,O'$) zinc (II) [2.023(3) Å] [34] and that in diaqua-bis(2-(indazol-1-yl)-2-thiazoline-N,N')-zinc(II) dinitrate [2.099(2) Å] [29].

In the molecular structure of the synthesized Zn(II) complex, intramolecular C7—H7···O2 contacts lead to the formation of seven-membered rings (Fig. 1) with a graph-set descriptor $S(7)$ [35]. In the crystal structure, water atom O1 in the molecule at (*x, y, z*) acts as a hydrogen-bond donor to atom O4 in the molecule at (−*x*, −*y*+2, −*z*+1) and (*x*, −*y*+3/2, *z*+1/2), so forming a $R_2^2(10)$ ring. In addition, atom N2 at (*x, y, z*) acts as a hydrogen-bond donor to atom O2 in the molecule at (*x, y*−1, *z*), so forming a second ring motif together with the O1—H1···O4 interaction, this time of $R_2^2(9)$ type. Propagation of these hydrogen-bonding motifs generates a chain of edge-fused rings running parallel to the [010] direction (Fig. 2). Full details of the hydrogen-bonding geometry are given in Table 2.

3.2. Optimized geometric structure

The isolated molecular structure from the crystal lattice of the synthesized Zn(II) complex was optimized in the DFT method by using B3LYP functional with a combination of 6-311++G(d,p) (for C,H, N, and O atoms) and SDD (for Zn atom) basis sets [15]. The optimized geometric structure is given in Fig. 3. Selected bond lengths and bond angle values from XRD data and theoretical calculations are listed in Table 3. Also, the other geometrical parameters of the optimized structure of the title complex were given in supplementary Table S1.

The Zn atom is coordinated from the N atom to the indazole molecule and the O atom to the nitrate groups. While the bond lengths of Zn1—N1 and Zn1—O3 bonds were obtained from XRD data of 2.0830 and 2.2416 Å, respectively, these values were found to be 2.0752 and 2.4196 Å in theoretical calculations. In addition, the Zn1—O1 bond length was determined as 2.0901 in the XRD data and was calculated at 2.2579 Å in theory. The bond angles of O1—Zn1—$O1^i$, O3—Zn1—$O3^i$, and N1—Zn1—$N1^i$ were found to be 180° in both experimental data and calculations. The bond angles of O1—Zn1—$N1^i$, O1—Zn1—N1, O3—Zn1—$N1^i$, and O3—Zn1—N1 are determined as 90.40, 89.60, 86.37, and 93.63° in XRD data, respectively, while the theoretical values corresponding to these experimental values were calculated at 90.97, 89.03, 91.72, and 88.27°. Only the experimental and theoretical data of $O1^i$—Zn1—O3 and O1—Zn1—O3 bond angles differed. The root mean square deviation (RMSD) values calculated for the experimental and calculated bond lengths and bond angles presented in Table 3 and Table S1 were found to be 0.0816/0.0864 and 9.43/11.07, respectively. According to this result obtained for bond lengths, we can say that the experimental and theoretical values are in harmony with each other. Experimental and theoretical bond angles of indazole rings are in good agreement with each other. However, there are differences between theoretical and experimental data for some angles formed by the Zn atom with nitrate groups, water molecules, and indazole rings. For this reason, the RMSD values obtained were high [36,37]. The reason for this difference can be explained as follows: the theoretical calculations are carried out on an isolated molecule in the gas phase, and there is no Coulombic interaction. However, the molecule in the crystal lattice is in Coulombic interaction [38].

Table 2
Hydrogen bonding geometry for the diaqua-bis(indazole-κN^2)bis(nitrato-κO) zinc(II) complex.

D—H···A	D—H (Å)	H···A (Å)	D···A (Å)	D—H···A (°)
C7—H7···O2	0.93	2.49	3.193(7)	133
N2—H6···O2[ii]	0.86	2.23	3.032(6)	156
O1—H1···O4[iii]	0.82(4)	1.98(4)	2.802(3)	177(4)
O1—H11···O4[iv]	0.80(4)	1.99(4)	2.782(3)	174(3)

Symmetry codes:
[ii] *x, y*−1, *z*;
[iii] −*x*, −*y*+2, −*z*+1;
[iv] *x*, −*y*+3/2, *z*+1/2.

3.3. Vibrational analysis

Vibrational calculations of the optimized geometric structure of the title complex were performed in the DFT method using the B3LYP functional with the combination of the 6-311++G(d,p) (for C, H, N, and O atoms) and SDD basis sets (for Zn atom) [15]. The theoretical and experimental frequency values were assigned according to a total energy distribution analysis (≥10%) calculated with the Veda program [39]. Selected frequency values are presented in Table 4. Other frequency values are listed in supplementary Table S2. Also, the calculated and recorded IR spectra were given in Fig. 4.

While the O-H stretching vibrations were calculated at 4024, 3825, and 3832 cm^{-1} for the synthesized Zn(II) complex, no value could be obtained for this vibration mode from the FT-IR spectrum. However, the observation of an expanding peak in the region between 3600 and 2800 cm^{-1} in the spectrum also confirms the presence of water molecules in the complex. The H-O-H bending vibrations of the H_2O molecule in complex structure are generally observed in the range of 1700-1500 cm^{-1} [40]. For the title complex, this vibration was observed as a weak peak at 1785 (w) cm^{-1} and was calculated at 1751 cm^{-1}. Also, the N-H stretching vibrations for the title complex could not be measured due to broadening in this region of the spectrum. The values of the calculated N-H stretching vibration are 3441 and 3445 cm^{-1} [41]. The N-H stretching vibrations of heterocyclic molecules are observed in the region of 3500–3000 cm^{-1}. In another study, it was reported that the N-H stretching vibration was observed at 3742 and 3148 cm^{-1} for the free indazole molecule and at 3753 and 3154 cm^{-1} for its silver nitrate complex in the FT-IR spectrum [10].

The CH group causes three different vibrations (stretching, in-plane bending, and out-of-plane bending). These vibrations occur in the regions of 3125–3000 [41], 1300-1000 [42], and 1000–750 cm^{-1} [43], respectively. For the synthesized Zn(II) complex, the C-H stretching vibration was observed at only 3283 (s) cm^{-1}, while these vibrational modes were theoretically calculated at 3260, 3197, 3191, 3181, and 3171 cm^{-1}. In the literature, these vibration values for the indazole molecule were observed at 3053 and 2917 cm^{-1} and at 3070 and 2930 cm^{-1} for its silver nitrate complex [10]. For the title complex, in-plane C-H bending vibrations were calculated at 1284, 1181, and 1149 cm, while they were only observed at 1137 (vw) cm^{-1} in the FT-IR spectrum. While out-of-plane C-H bending vibrations were calculated at 1001, 997, 995, 971, 964, 858, and 723 cm^{-1}, they were observed at 962 (s) and 716 (vw) cm^{-1}.

The C-C stretching vibrations for the athomatic rings of heterocyclic molecules are generally observed in the shade in the range of 1650–1200 cm^{-1} [44]. The C-C stretching vibrations for the synthesized Zn(II) complex were measured at 1634 (vs) and 1387 (w) cm^{-1} in the FT-IR spectrum. The theoretical C-C stretching vibrations corresponding to these experimental values are 1628/1631 and 1399/1396 cm^{-1}, respectively. In addition, C-C stretching vibrations were determined at 1674, 1555, 1542, 1477, and 1284 cm^{-1} in theoretical calculations. The C-C stretching vibrations for the silver nitrate complex of the indazole molecule were reported at 1630, 1508, 1120, and 999 cm^{-1} in the previous study [10].

The C=N stretching vibrations are observed in the region between 1672 and 1566 cm^{-1} [45,46]. These stretching vibrations for the synthesized Zn(II) complex were observed at 1516 (m) and 1419 (w) cm and were also calculated at 1519 and 1439 cm^{-1}. In a previous study, the C=N stretching vibration was observed at 1477 cm^{-1} for the indazole

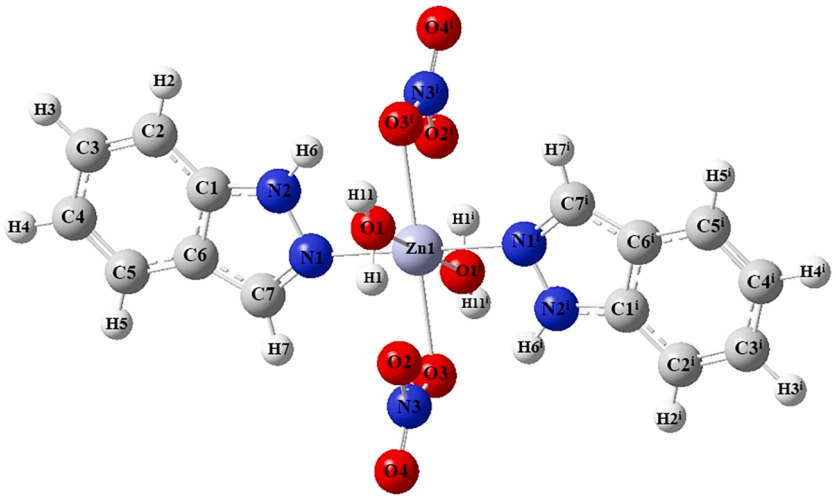

Fig. 3. Optimized molecular structure of the diaqua-bis(indazole-κN^2)bis(nitrato-κO)zinc(II) complex.

Table 3
Selected experimental and calculated bond lenghts and bond angles of the diaqua-bis(indazole-κN^2)bis(nitrato-κO)zinc(II) complex.

Parameters		
Bond lengths (Å)	Calculated	XRD
Zn1—O1	2.2579	2.0901(17)
Zn1—O3	2.4196	2.2416(15)
Zn1—N1	2.0752	2.0830(19)
RMSD:	0.0816/0.0864	
Bond angles (°)		
O1—Zn1—O1^i	180.00	180.00
O3—Zn1—O3^i	180.00	180.00
N1—Zn1—N1^i	180.00	180.00
O1—Zn1—N1^i	90.97	90.40(8)
O1—Zn1—N1	89.03	89.60(8)
O3—Zn1—N1^i	91.72	86.37(7)
O3—Zn1—N1	88.27	93.63(7)
O1^i—Zn1—O3	61.65	83.95(7)
O1—Zn1—O3	61.65	96.05(7)
RMSD:	9.43/11.07	

Selected geometric parameters for the diaqua-bis(indazole-κN^2)bis(nitrato-κO) zinc(II) complex. Symmetry code:
^{i} $-x, -y+1, -z+1$.

molecule [47]. Also, this vibration value shift to two different values (1516 and 1419 cm^{-1}) indicates that the Zn atom is coordinated with the N atoms of the indazole molecules in the complex.

In inorganic compounds, stretching vibrations of the nitrate group are seen in the region of 1650-1221 cm^{-1} [48]. The band observed at 1317 (vs) cm^{-1} in the Ir spectrum of the synthesized title complex and not found in the spectrum of the free indazole molecule [10] is N-O stretching vibration, which confirms the presence of the NO3$^-$ group. Another O-N stretching vibration was observed at 1075 (s) cm^{-1}, and the values of this stretching vibration were found at 1310/1316, 1279/1276, 1268, and 1065 cm^{-1} in theoretical calculations. In another study, $[Zn_2(L)_2(NO_3)_2]$ (L: 2,6-bis((E)-((furan-2-ylmethyl)imino) methyl)-4 methylphenol) complex was synthesized. The N-O asymmetric stretching vibration of the nitrate groups of this synthesized complex was also observed at 1329 cm^{-1} [49]. In a study in the literature, the $[Zn•2CO(NH_2)_2•(NO_3)_2]•2H_2O$ complex was synthesized and characterized by the Ir spectrum, and it was reported that asymmetric N-O stretching vibrations were observed at 1317 and 1047 cm^{-1} in the Ir spectrum of this complex [50]. Additionally, in some nitrate compounds, N=O stretching modes in the nitrate group are observed in the region between 1460-1672 cm^{-1} [36]. This stretching vibration for the title complex could not be observed in the experimental FT-IR spectrum, but was calculated at 1555 and 1542 cm^{-1} in theoretical calculations.

The Zn-N stretching vibrations of the synthesized Zn(II) complex were observed at 459 (w) and 150 (w) cm^{-1} in the IR spectrum, while the theoretical values corresponding to these values were calculated at 469 and 164 cm^{-1}. In a study in the literature, Zn(II) complexes of Schiff base tetradentate macrocyclic ligands were synthesized, and IR spectrum analyses were performed to characterize the structures obtained. In this study, it was reported that the weak low-frequency bands observed in the 420–450 cm^{-1} region belong to the stretching vibrations caused by the formation of the Zn–N bond [51]. In another study, Schiff base ligand (L) was obtained by mixing the solutions of N1-(2-(2-aminoethylamino)ethyl)ethane-1,2-diamine and (E)-3-(2-nitrophenyl). Then, the Zn(II) complex of this ligand was synthesized. The Zn-N stretching vibration for the $ZnL(NO_3)_2$ complex has also been reported at 431 cm^{-1} [52].

The Zn-$O_{nitrate}$ stretching vibrations of the synthesized Zn(II) complex were observed at 353 and 278 cm^{-1}. Also, the Zn-O_{water} stretching vibrations were recorded at 325 and 204 cm^{-1}. The calculated vibration values of this vibration were found to be 355, 273, 321, 207, and 185 cm^{-1}. A study in the literature [Zn(6-mbipy)(η^2-$NO_3)_2$], [Zn(6,6′-dmbipy)(η^2-$NO_3)_2$] and [Zn(5,5′- dmbipy) (η^2-$NO_3)_2(H_2O)_2$]$(NO_3).H_2O$ complexes were synthesized, and their spectroscopic characterizations were performed. In this study, Zn–$O_{nitrate}$ stretching vibrations for all three complexes were measured at 365 and 340 cm^{-1}, 343 and 310 cm^{-1}, and 335 and 314 cm^{-1}, respectively. Also, Zn–O_{water} stretching vibrations of the [Zn(5,5′- dmbipy) (η^2-$NO_3)_2(H_2O)_2$]$(NO_3).H_2O$ complex were recored 360 cm^{-1} [53].

To show the agreement between experimental and theoretical wavenumbers, a correlation graph was drawn (supplementary Fig. S1), and the R^2 value was calculated. The R^2 value was found to be 0.9998. This result shows that the experimental and theoretical wavenumbers are quite compatible with each other.

3.4. HOMO-LUMO molecular orbital analysis

The energy difference between the highest occupied molecular orbital (HOMO) and the lowest unoccupied molecular orbital (LUMO) is defined as the lowest possible excitation energy of a molecule [54]. The difference between the HOMO-LUMO energy gap is used to determine the chemical stability and electrical properties of molecules. The smaller this energy gap, the greater its polarizability, and the molecule tends to have high chemical reactivity and low kinetic stability [55]. Also, other quantum chemical properties can be calculated with the equations given below using the HOMO and LUMO values, known as the electron-donating and electron-accepting abilities of a molecule [56].

Table 4
Selected experimental and theoretical wavenumbers with their assigments according to total energy distrubition (%) of the diaqua-bis(indazole-κN^2)bis(nitrato-κO)zinc(II) complex.

Experimental	Calculated		Assignments
IR	IR	I_{IR}[a]	TED[b]
62m	61/64	0.13	$15\Gamma_{CNZnO} + 20\Gamma_{NNZnO} + 12\Gamma_{HOZnN} + 12\Gamma_{HOZnO}$
72s	82/86	0.00	$17\Gamma_{CNZnO}$
98m	104	4.48	$10\Gamma_{CNZnO}$
150w	164	0.00	$10\upsilon_{ZnN} + 14\Gamma_{HOZnN} + 14\Gamma_{HOZnO}$
173vw	177	0.41	$13\Gamma_{HOZnN} + 14\Gamma_{HOZnO}$
	185	0.00	$10\upsilon_{ZnO} + 15\Gamma_{HOZnN} + 11\Gamma_{HOZnO}$
204m	207	8.32	$10\upsilon_{ZnO} + 17\Gamma_{HOZnN} + 15\Gamma_{HOZnO}$
248w	242	0.54	$10\Gamma_{HOZnN} + 10\Gamma_{HOZnO}$
278w	273	0.57	$10\upsilon_{ZnO} + 15\Gamma_{CCCC} + 18\Gamma_{CCCH} + 10\Gamma_{HOZnN} + 10\Gamma_{HOZnO}$
304w	300	0.00	$15\Gamma_{CCCC} + 13\Gamma_{CCCH} + 10\Gamma_{CNZnO}$
325w	321	0.00	$14\upsilon_{ZnO} + 10\Gamma_{HOZnN} + 10\Gamma_{HOZnO}$
353w	355	0.35	$13\upsilon_{ZnO} + 10\Gamma_{HOZnN} + 10\Gamma_{HOZnO}$
377w	386	1.42	$10\Gamma_{CCCC} + 10\Gamma_{HOZnO}$
425	427	3.20	$25\Gamma_{CCCC} + 18\Gamma_{CCCH}$
459w	469	3.82	$10\upsilon_{ZnN} + 10\Gamma_{HOZnO}$
552w	544	1.00	$25\Gamma_{CCCC} + 18\Gamma_{CCCH}$
572vw	572	0.00	$23\upsilon_{CC} + 10\delta_{CCH} + 10\Gamma_{HOZnN} + 10\Gamma_{HOZnO}$
591w	587/592	1.11	$12\Gamma_{HOZnN} + 13\Gamma_{HOZnO}$
615vw	626	2.24	$14\Gamma_{CCCC} + 26\Gamma_{CCCH} + 17\Gamma_{HCCH}$
680m	691	10.38	$32\Gamma_{HOZnN} + 31\Gamma_{HOZnO}$
716vw	723	1.00	$12\Gamma_{CCCH} + 12\Gamma_{HOZnN} + 12\Gamma_{HOZnO}$
740w	746	2.00	$69\delta_{ONO}$
777m	777	4.02	$74\delta_{ONO}$
817m	805/811	5.34	$64\delta_{HOZn}$
826w	833/836	4.88	$93\Gamma_{OOON}$
899m	889	11.02	$14\Gamma_{CCNH}$
962s	964	15.03	$13\Gamma_{CCCC} + 27\Gamma_{CCCH} + 17\Gamma_{HCCH}$
1005m	1012	9.48	$12\Gamma_{HOZnN} + 12\Gamma_{HOZnO}$
1040m	1029/1032	1.56	$10\Gamma_{CCCC} + 20\Gamma_{CCCH} + 13\Gamma_{HCCH}$
1075s	1065	35.36	$25\upsilon_{ON} + 10\Gamma_{HOZnN} + 10\Gamma_{HOZnO}$
1095m	1100	11.60	$18\Gamma_{CCCH} + 16\Gamma_{HOZnN} + 15\Gamma_{HOZnO}$
1137vw	1149	0.43	$10\upsilon_{CC} + 16\delta_{CCH}$
1247m	1247/1251	8.64	$10\upsilon_{CC} + 32\delta_{CCH}$
1317vs	1310/1316	15.27	$20\upsilon_{ON}$
1387w	1396/1399	2.89	$41\upsilon_{CC} + 32\delta_{CCH}$
1419w	1439	1.00	$20\upsilon_{CN} + 12\delta_{CNH} + 32\delta_{CCH}$
1516m	1519	5.41	$12\upsilon_{CN} + 10\delta_{CCH}$
1634vs	1628/1631	40.82	$26\upsilon_{CC} + 12\delta_{CCC} + 13\delta_{CCH}$
1785w	1751	2.29	$23\delta_{HOH} + 13\delta_{HOZn}$
3283s	3260	25.02	$48\upsilon_{CH} + 19\delta_{CCH}$
-	3441/3445	100.00	$32\upsilon_{NH} + 51\delta_{CNH}$
-	3825/3832	14.23	$46\upsilon_{OH} + 23\Gamma_{HOZnN} + 23\Gamma_{HOZnO}$
-	4024	0.00	$48\upsilon_{OH} + 16\Gamma_{HOZnN} + 15\Gamma_{HOZnO}$

υ: stretching, δ: in-plane bending, Γ: torsion, s: strong, m: medium, w: weak, v: very.

[a] Relative absorption intensities normalized with highest peak absorption equal to 100.

[b] Total energy distribution level (TED) less than 10% are not shown.

$$I = -E_{HOMO}\ \textbf{ionizationpotantial} \quad (1)$$

$$A = -E_{LUMO}\ \textbf{electronaffinity} \quad (2)$$

$$\eta = (-E_{HOMO} + E_{LUMO})/2\ \textbf{globalhardness} \quad (3)$$

$$\mu_c = (E_{HOMO} + E_{LUMO})/2\ \textbf{chemicalpotential} \quad (4)$$

$$\chi = -\mu_c\ \textbf{electronegativity} \quad (5)$$

$$\sigma = 1/\eta\ globalsoftnes \quad (6)$$

Global hardness is a reactivity index that evaluates the degree of chemical reactivity that stabilizes the system as a result of adding a charge to the molecule. Chemical potential is a general index of reactivity related to charge transfer from a system with a higher chemical potential to a system with a lower chemical potential. Electronegativity, which is the negative value of chemical potential, is the power to attract electrons [57].

The energy values of the quantum chemical properties of the title complex were calculated in the DFT method using the B3LYP functional with a combination of the 6-311++g(d,p) (for light atoms (C, H, N, and O)) and the SDD basis set (for the heavy atom (Zn)). The energy values of the quantum chemical properties of the synthesized Zn(II) complex are listed in Table 5.

The energy values of the HOMO and LUMO orbitals were calculated as -6.51 and -1.77 eV, respectively. The energy gap between these two orbitals was found to be 4.74 eV. Global hardness and global softness values were determined as 2.37 and 0.42 eV, respectively. These results show that the synthesized Zn(II) complex has low reactivity and high chemical stability. When these results are evaluated with the studies in the literature, it is concluded that this synthesized complex has a hard structure [58]. In the other study, the energy gap, global hardness, and global softness values for the free indazole molecule have been reported as 5.17, 2.58, and 0.38 eV, respectively [10]. According to these results, the synthesized title complex has a more reactive structure than the free ligand. The electron distribution visualizations of the HOMO and LUMO orbitals are given in Fig. 5. HOMO has been distributed on the Zn atom, NO_3, and H_2O groups with the pyrazole rings of the indazole ligands of the synthesized complex. On the other hand, LUMO showed distribution over the indazole ligands in the complex. In other words, this figure shows how the electronic transition occurs between the highest occupied molecular orbital (HOMO) and the lowest unoccupied molecular orbital (LUMO) and how the electrons are distributed as a result of charge transfer.

3.5. UV-Vis spectral analysis

The UV-Vis absorption spectrum of the synthesized Zn(II) complex was recorded in the range of 190–1100 nm in ethanol solution, and theoretical calculations were performed at the TD-DFT/B3LYP/SDD level of theory in DMSO solution [18]. The experimental UV-Vis absorption spectrum is presented in Fig. 6, while wavelengths, excitation energy, oscillator strength, and major contribution values obtained from theoretical calculations are presented in Table 6. A broad absorption band at 283 nm and a lower-intensity absorption band at 239 nm were observed in the experimental spectrum for the title complex. The energy values for these absorption bands are 4.38 and 5.19 eV, respectively. In theoretical calculations, the wavelength was calculated at 268 nm with an energy value of 4.62 eV resulting from the HOMO-1/Lumo+2 and HOMO/LUMO+3 transitions. This wavelength corresponds to 283 nm in the experimental spectrum. Also, another wavelength was calculated at 239 nm in theoretical calculations. The energy gap value for the synthesized Zn(II) complex was calculated at 4.74 eV. It is also very compatible with the energy of the UV-Vis absorption band observed at 283 nm in the experimental spectrum.

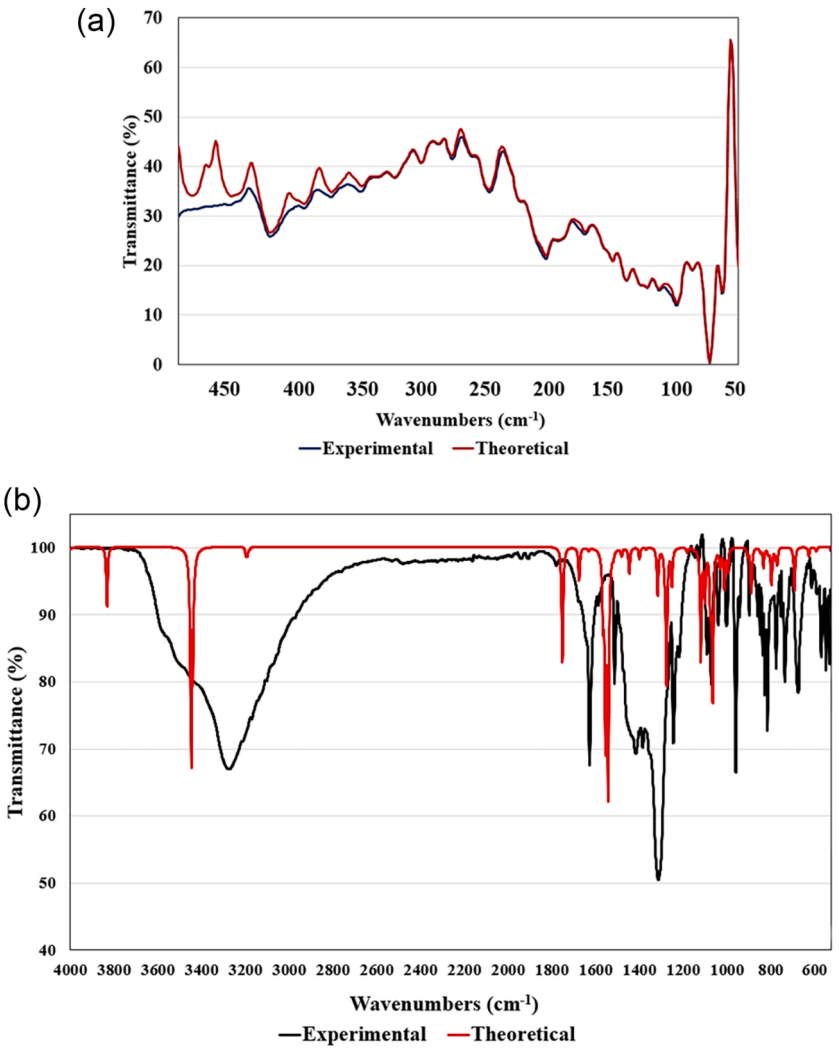

Fig 4. Experimental Far-IR (a) and FT-IR spectra of the diaqua-bis(indazole-κN^2)bis(nitrato-κO)zinc(II) complex

Table 5
The energy values of the quantum chemical properties of the diaqua-bis(indazole-κN^2)bis(nitrato-κO)zinc(II) complex.

Molecular Orbitals	Energy (eV)		Energy gap (eV)	Ionization potential (I) (eV)	Electron affinity (A) (eV)	Global hardness (η) (eV)	Electronegativity (χ) (eV)	Chemical potential (μ_c) (eV)	Global softness (σ) (eV^{-1})	Global electrophilicity (ω) (eV)
H	-6.51	ΔE_{H-L}	4.74	6.51	1.77	2.37	4.14	-4.14	0.42	3.61
L	-1.77									
H-1	-6.76	$\Delta E_{H_{-1}-L_{+1}}$	4.99	6.76	1.76	2.50	4.26	-4.26	0.40	3.63
L+1	-1.76									
H-2	-6.77	$\Delta E_{H_{-2}-L_{+2}}$	5.32	6.77	1.45	2.66	4.11	-4.11	0.38	3.18
L+2	-1.45									

H: HOMO, L: LUMO

3.6. Hirshfeld surface analyses

Using the Crystal Explorer 17 package program, Hirshfeld surface and 2D finger drawing analyses were performed to determine intermolecular interactions within the crystal structure [59,60]. In the analysis, the CIF file of the synthesized complex was used as an input file. de is defined as the distance from a certain point on the surface to the nearest atom inside, while di is the distance to the closest atom outside. The normalized surface distance (dnorm) is obtained from the$d_{norm} = \frac{d_i - r_i^{VdW}}{r_i^{VdW}} + \frac{d_e - r_e^{VdW}}{r_e^{VdW}}$ equation as a function of the de and di values and the Van der Waals radius values of the atoms. [61–63]. Hirshfeld surface graphics prepared according to the d_{norm}, d_i, and d_e properties are presented in Fig. 7. The red-colored areas on the dnorm surface plot correspond to the O-H contacts that contribute the most to the Hirshfeld surface. According to the fingerprint drawing graphics presented in Fig. 8, it was seen that 36.7% came to the Hirshfeld surfaces from O-H/H-O interactions. These interactions are represented by the blue spike regions on the lower left and right. Other top contributions to the Hirshfeld surface come from the H-H/H-H interactions represented by the blue spike in the middle region with 30.9% and the C-H/H-C interactions represented by the upper right and left regions with 16.2%.

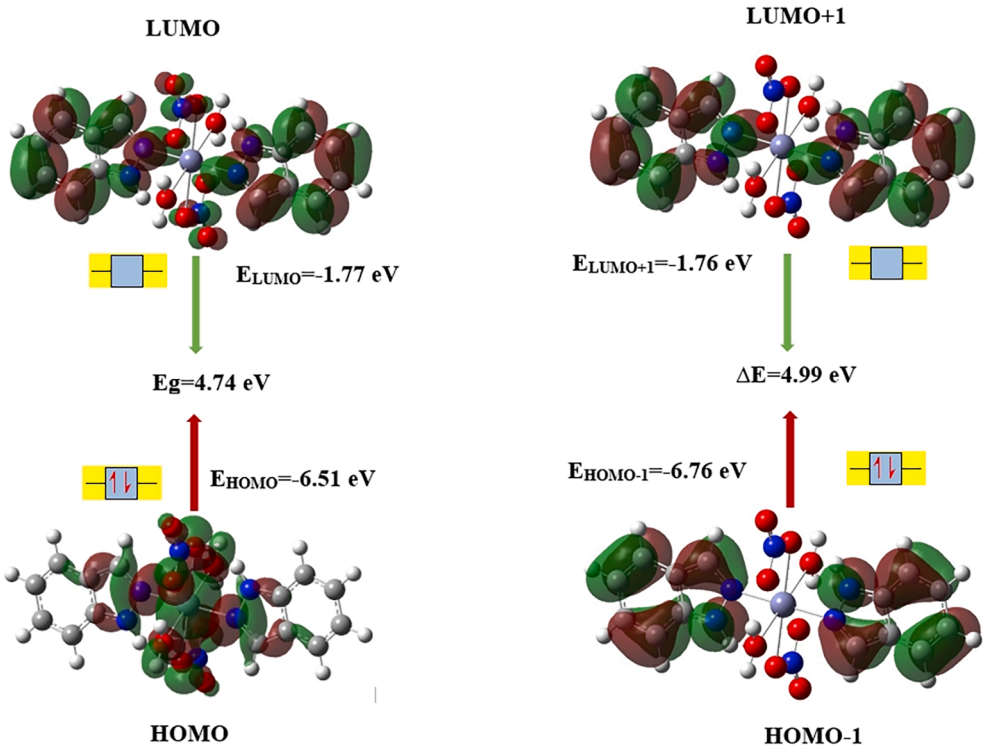

Fig. 5. HOMO-LUMO distrubitions of the diaqua-bis(indazole-κN^2)bis(nitrato-κO)zinc(II) complex.

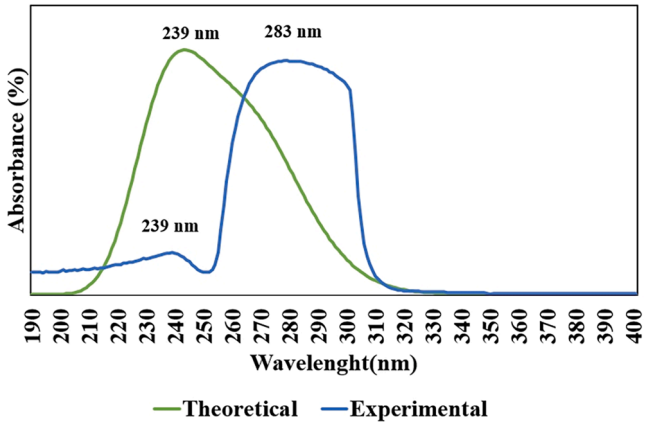

Fig. 6. The experimental UV-Vis absorbsion spectrum of the diaqua-bis(indazole-κN^2)bis(nitrato-κO)zinc(II) complex.

Table 6
Experimental and calculated UV-Vis wavelength (λ), excitation energy (eV) and oscillator strength (f) for the diaqua-bis(indazole-κN^2)bis(nitrato-κO)zinc(II) complex.

Experimental	Theoretical				
λ (nm)	λ (nm)	E (eV)	f	Symmetry	Major Contributions
283	268	4.62	0.3496	Singlet-A	HOMO-1 → LUMO+2 HOMO → LUMO+3
239	239	5.19	0.4913	Singlet-A	HOMO-2 → LUMO+2 HOMO-3 → LUMO

3.7. MEP analysis

The molecular electrostatic potential surface (MEP) map is a tool used to predict the electrophilic and nucleophilic regions of a molecule and provides extremely important information about its chemical stability and reactivity [64]. Electron densities are represented by different colors on the map. The red color represents the electron-rich region, while the blue color represents the electron-poor region. Green represents neutral regions, and yellow represents slightly electron-rich regions [65,66]. The MEP map of the optimized complex structure created based on electron charge is presented in Fig. 9. According to this map, O3, O4, O3′, and O4′ atoms of complex nitrate groups are located in the red-colored electrophilic region. The N1 and N1′ atoms in the pyrazole ring of the indazole molecules of the synthesized complex are located in the blue-colored nucleophilic region. In addition, the carbon atoms in the benzene ring are located in the yellow-colored region, that is, in the slightly electron-rich region of this map.

In the MEP map created for the indazole molecule, the red (electrophilic) region is on the N atom that has not bonded with the H atom. The fact that the N1 and N2 atoms of the synthesized complex are in the blue-colored region (positive) is an indication that they are coordinated with the Zn atom. Also, the MEP map gives similar results to the HOMO distribution map presented in Fig. 5. In both maps, the most electron-dense regions are around the oxygen atoms of the nitrate groups.

3.8. Fukui Function analysis

Fukui functions are an important tool used to define the electrophilic and nucleophilic regions of a molecule, or, in other words, to determine the local reactivity of the atoms of the molecule [67]. The Fukui functions for the neutral, cationic, and anionic states of the synthesized Zn (II) complex were obtained from the Hirshfeld charges calculated in the DFT method using the B3LYP functional and a combination of 6-311++g(d,p) and SDD basis sets with the following equations:

$$f_k^0 = (1/2)[q_k(N+1) - q_k(N-1)] \quad \textbf{forneutralattack} \qquad (7)$$

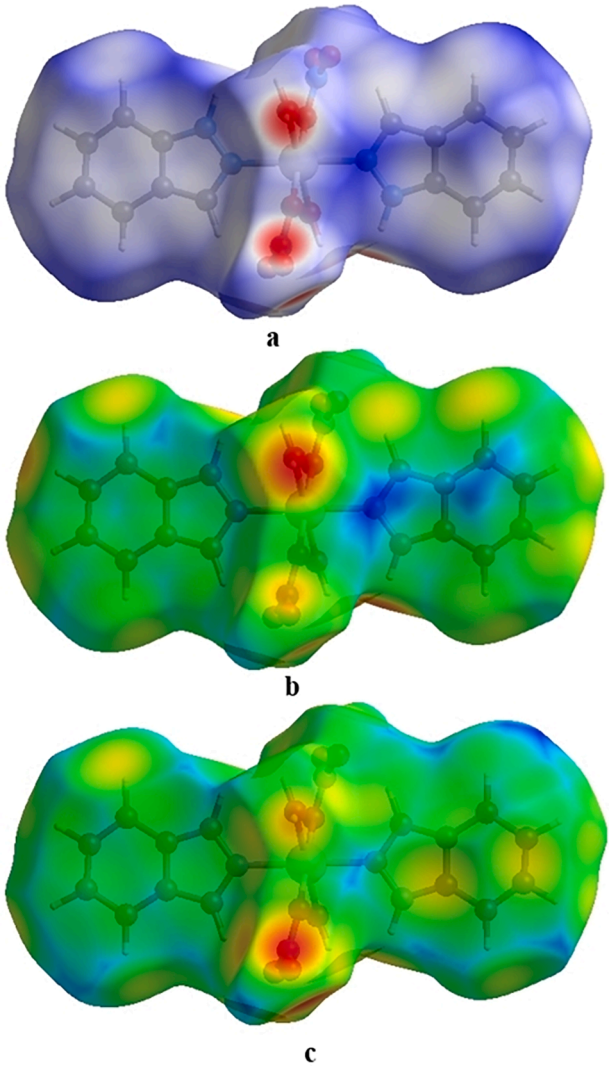

Fig. 7. The Hirshfeld surfaces mapped over d_{norm} (a), d_i (b), and d_e (c) of the diaqua-bis(indazole-κN^2)bis(nitrato-κO)zinc(II) complex.

$$f_k^+ = q_k(N+1) - q_k(N)\ \textbf{fornucleophilicattack} \quad (8)$$

$$f_k^- = q_k(N) - q_k(N-1)\ \textbf{forelectrophilikattack} \quad (9)$$

In these equations, qkN, qk(N+1), and qk(N-1) are the atomic charges at the r position in a neutral, anionic, or cationic system [68]. The dual descriptor Δf(r) provides the most accurate estimation of electrophilicity and nucleophilicity, creating a clear distinction between active sites in the molecule [69].

$$\Delta f(r) = f^+(r) - f^-(r) \quad (10)$$

The sign of this calculated dual descriptor is important to predict electrophilic and nucleophilic regions. If $\Delta f(r) > 0$, the site is likely to be attacked by nucleophiles, while if $\Delta f(r) < 0$, the site is likely to be attacked by electrophiles [70]. The Fukui function values of the title complex are presented in supplementary Table S3. Also, the dual descriptor image created with the Multiwfn program is presented in supplementary supplementary Fig. S2 [21]. In this image, blue indicates electrophilic regions (favorite for nucleophilic attacks), while green indicates nucleophilic regions (favorite for electrophilic attacks).

When we examine supplementary Fig. S1, the O atoms of nitrate groups and the N2, C2, C4, and C7 atoms of the indazole molecule (with their mirror-symmetry counterpart atoms) are in the blue region. That is, these atoms behave as electrophilic and are preferred for nucleophilic attacks.

Also, Fukui functions calculated for Hirshfeld charges (see in supplementary Table S3) with the Gaussian 09 package program are compatible with the image in supplementary Fig. S2. In the dual descriptor obtained by Fukui functions, O3, O4, $O3^i$, and $O4^i$ atoms of nitrate groups, N1, N2, $N1^i$, and $N2^i$ atoms, and C2, C4, C7, $C2^i$, $C4^i$, and $C7^i$ atoms exhibit electrophilic behavior. All the obtained results for Fukui functions also confirm the MEP map.

3.9. Charge analysis

Charge analyses are used to predict the behavior of a chemical system in electrophilic and nucleophilic reactions in a molecule [71,72]. In this study, the charge values of each atom of the optimized structure of the synthesized Zn(II) complex were calculated by atomic polar tensor (APT), Hirshfeld, and natural bond orbital (NBO) charge analysis. Calculations were performed in the DFT method using the B3LYP function and the combination of 6-311++G(d,p) and SDD basis sets. The

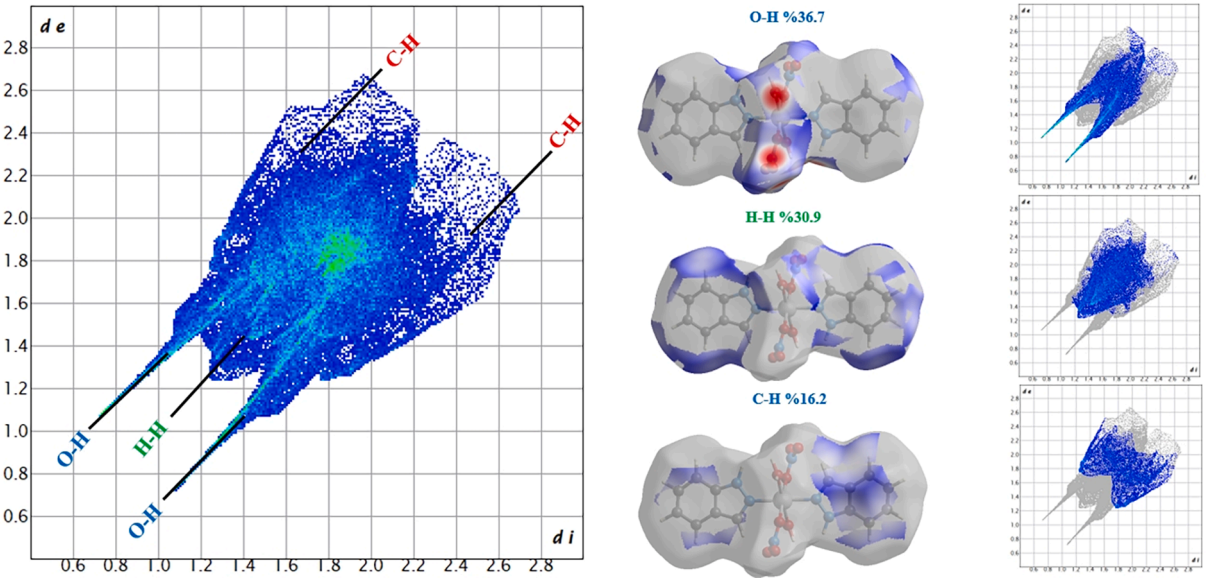

Fig. 8. Two-dimensional fingerprint plots of the diaqua-bis(indazole-κN^2)bis(nitrato-κO)zinc(II) complex.

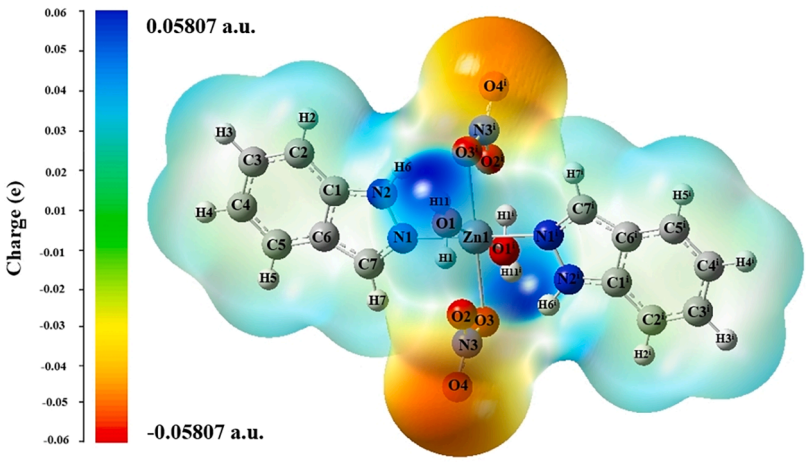

Fig. 9. Electrostatic potential surface map of the diaqua-bis(indazole-κN^2)bis(nitrato-κO)zinc(II) complex created using the DFT method. Isodensity value is 0.0004.

calculated charge values are presented in supplementary Table S4 and given in supplementary Fig. S3.

According to all three charge analysis methods, the O atoms of the NO_3 group and the N atoms of the indazole molecule have negative values. In addition, the charge values of the C1, C1i, C7, and C7i atoms in the complex are also negative. Zn1, N3, and N3i are the atoms that have the highest positive charge. The results obtained from the charge analyses performed are similar to those obtained from the Fukui functions and the MEP map.

3.10. Non-covalent intermolecular interactions

3.10.1. Natural bond analysis (NBO)

The electron density distributions in the atoms of molecular systems were found using NBO analysis [73]. Additionally, it has been used to determine which intra- and intermolecular interactions cause the system under study to stabilize [74]. The NBO investigation of the Zn(II) complex showed the interactions between the donor NBOi and acceptor NBOj orbitals, which are listed in Table 7. Using second-order perturbation theory, the interaction between non-Lewis acceptor and Lewis-type donor NBOs is important for the synthesized complex. The higher second-order perturbation interaction energy $E^{(2)}$ suggests that molecular electron donors and acceptors in the molecular system can interact very well. Considering the calculated second-order interaction energy values of metal-ligand bonds and H-bonds in the examined complex, the maximum energy $E^{(2)}$ value was 32.64 kcal/mol, which corresponds to LP(1) N→ LP*(6) Zn. As can be seen in Table 7, N16 (N1), N19 (N1′), and O39 (O3) and O42 (O3′) atoms have the most negative atomic charges. These electronic redistributions may be attributed to the excited state intramolecular proton transfer process induced by the hydrogen atom transfers from oxygen to nitrogen atom (formation of N–H…O hydrogen bonding). In addition, we can notice that the hydrogen atoms have the most positive atomic charges in the Zn(II) complex. According to NBO analysis, an intramolecular interaction is observed between the nitrogen atoms of the pyrazole ring and the nitrat group (N_{19}-H_{31}….O_{39} and N_{16}-H_{27}….O_{42}).

3.10.2. Atoms in molecules analysis (AIM)

The electron density distribution of a molecular system can be used by the well-known quantum theory of atoms in molecules (QTAIM) approach to physically represent the forces acting on the molecular system [75]. This method is commonly used to calculate interatomic and intraatomic interactions. The calculated topological parameters that provide a lot of information about the properties of RCPs and BCPs of the synthesized complex are listed in Table 8, whereas the graphical representation of AIM analysis is illustrated in supplementary Fig. S4.

According to AIM theory, the properties of the bonds, especially the hydrogen bonds, are confirmed by three criteria proposed by Koch and Popelier [76]: (i) The presence of a BCP between the acceptor group and the hydrogen atom of the donor group confirms the existence of a hydrogen bond. (ii) The value of ρ(r) at the BCP point should be low and located in the range 0.0020–0.0400 a.u. (iii) The value of $\nabla^2\rho(r)$ should be positive and located in the range 0.0240–0.1390 a.u. [77]. The AIM topological analysis in Table 8 shows that the N-H···O hydrogen bonds of our crystal are considered weak hydrogen bonds ($\nabla^2\rho$ (r) > 0 and H (r) > 0), and $\nabla^2\rho(r)$ and ρ(r) indicate that the values are within the allowed range [78]. The electron density and the Laplacian parameters are important in defining the nature of interactions. Furthermore, for the N19-H31...O39 and N16-H27...O42 bonds in the indazole molecule, the ratio $|V(r)|/G(r)>1$ suggests that a local concentration of the charge stabilizes the interaction. The interaction energy E_{int} (−27.974 kcal/mol) indicates a strong interaction between the nitrate group and the N19 and N16 atoms of the pyrazole ring. The Zn-N18 and Zn-N17 bonds are found to be stretched. It was found that $\nabla^2\rho(r) > 0$ and H(r) < 0,

Table 7
Second-Order perturbation theory analysis of Fock matrix in NBO corresponding to the selected charge transfer interactions of the complex

H-bonds	donor→acceptor	$E^{(2)}(kcal/mol)^a$	$\varepsilon_j - \varepsilon_i(a.u.)^b$	$F(i.\ j)(a.u.)^c$
N_{19}-H_{31}….O_{39}	$LP(1)(O_{39})\rightarrow\sigma^*(N_{19} - H_{31})$	1.02	1.03	0.029
N_{16}-H_{27}….O_{42}	$LP(2)(O_{42})\rightarrow\sigma^*(N_{16} - H_{27})$	2.19	0.88	0.040
Metal-ligand bonds	donor→acceptor	$E^{(2)}(kcal/mol)^a$	$\varepsilon_j - \varepsilon_i(a.u.)^b$	$F(i.\ j)(a.u.)^c$
	$LP(1)(N_{18})\rightarrow LP^*(6)(Zn_{45})$	32.64	0.65	0.132
	$LP(1)(N_{17})\rightarrow LP^*(6)(Zn_{45})$	32.64	0.65	0.132

σ : sigma bonds, *LP*: lone pairs, LP*: anti-lone pairs
[a] $E^{(2)}$ means energy of hyper conjugative interactions.
[b] Energy difference between donor and acceptor i and j NBO orbitals.
[c] $F_{(i,j)}$ is the Fock matrix element between i and j NBO orbitals

Table 8
Topological parameters of Zn(I) complex.

Interactions	ρ(r)	$\nabla^2\rho(r)$	H(r)	G(r)	V(r)	E_{int} (kcal/mol)	V(r)/G(r)
Zn-N_{18}	0.06841	0.33054	-0.00326	0.08589	-0.08916	-27.974	1.03807
Zn-N_{17}	0.06842	0.33056	-0.00326	0.08590	-0.08916	-27.974	1.03795
O_{42}….O_{43}	0.02503	0.12666	0.00410	0.02755	-0.02345	-7.357	0.85118
O_{39}….O_{38}	0.02503	0.12667	0.00401	0.02756	-0.02345	-7.357	0.85087
N_{19}-H_{31}….O_{39}	0.03032	0.10687	0.00117	0.02554	-0.02437	-7.646	0.95419
N_{16}-H_{27}….O_{42}	0.03032	0.10685	0.00117	0.02553	-0.02436	-7.642	0.95417
N_{20}-O_{41}….H_{25}	0.02812	0.12861	0.00306	0.02908	-0.02602	-8.163	0.89477
N_{15}-O_{40}….H_{35}	0.02811	0.12858	0.00306	0.02907	-0.02601	-8.160	0.89474
N_{20}-O_{42}….O_{43}	0.02503	0.12666	0.00410	0.02755	-0.02345	-7.357	0.85118
NRCP1	0.01258	0.05381	0.00122	0.01222	-0.01100	-3.451	0.90016
NRCP2	0.01258	0.05381	0.00122	0.01222	-0.01100	-3.451	0.90016

D (Á): Distance; ρ(r) (a.u.): Density of electrons; $\nabla^2\rho(r)$ (a.u): Laplacian of electron density; V(r) (a.u): Potential energy density; (Eint) (kcal/mol): Interaction energy, NRCP: new ring critical poin

which were used as descriptives to investigate the nature and strength of these interactions. These findings characterize the closed-shell interactions, including the extremely polar covalent character of the examined bonds [79]. The critical point of the ligand-H2O is of the hydrogen bonding type, with $H > 0$ and $\nabla^2(\rho) > 0$, which seems to be non-covalent. Furthermore, the presence of new ring critical points, NRCP1 and NRCP2 cycles, which are created by interactions between the organic group and the inorganic anion via hydrogen bonds, can be detected in a molecular system using the AIM analysis.

3.10.3. Non-covalent interaction-reduced density gradient (NCI-RDG)

The reduced density gradient (RDG) is a dimensionless primary quantity derived from the density's first derivative. The study of non-covalent interactions in the form of a scatter plot of the RDG with respect to the real space function $Sign(\lambda_2)\rho$ reveals the second-highest Eigenvalue of the Hessian matrix λ_2 of the electron density [0-S0022286023000479]. The 3D visualization of the NCI interaction given in supplementary Fig. S5 is mapped to a color coding scheme as follows: blue-green-red, which represents $Sign(\lambda_2)\rho > 0$ (bonds or halogen bonds), $sign(\lambda_2)\rho < 0$ (van der Waals interactions), and $Sign(\lambda_2)\rho = 0$ (steric repulsions) [80]. The steric effect and repulsive interactions observed in the center of aromatic rings are depicted in the 3D representation; these are related to π-π stacking interactions, which are depicted as the red area in the RDG plot. Also, Van der Waals interactions were located between (H31, O39), (H27, O42), (H25, O41), (H35, O40), and (H43, O42). The RDG results were clearly in agreement with the QTAIM and NBO findings.

3.10.4. ELF and LOL analyses

Electron localization function (ELF) and localized orbital locator (LOL) surface analyses of the synthesized Zn(II) complex were performed using the Multiwfn program [20]. The ELF and LOL surface maps created for the title complex are given in supplementary Fig. S6. These surface maps reveal the possibility of finding an electron pair on the molecular surface and are related to kinetic energy density. However, the ELF map is created depending on the electron pair density, while the LOL map is created during the overlapping of the orbitals due to the gradient of the localized orbitals [81]. ELF maps are designed in the range of 0.0–1.0. It is expected that bonding and non-bonding localized electrons are in the region of 0.5–1.0, and delocalized electrons are expected to be in the region of 0.0-0–5 [82]. In Fig. S6a, the red color surrounding the hydrogen atoms indicates the presence of bonding and non-bonding localized electrons. The blue ring around the carbon and nitrogen atoms of the indazole molecule indicates the presence of delocalized electrons. Similar results were obtained from the LOL map given in supplementary Fig. S6b.

3.11. Thermodynamic properties

The thermodynamic parameters of the Zn(II) complex, such as enthalpy change (ΔH), entropy (S), and heat capacity (Cp), were calculated using theoretical information derived from vibrational analysis by the DFT method in the gas phase. These thermodynamic data were evaluated in the temperature range of 100 K to 500 K, and the results are given in Table 9. Looking at the results obtained, it was observed that thermodynamic parameters (S, Cp, and H) increased as the temperature increased. This previous research suggests that this is to be predicted [83]. Thermodynamic properties provide information about the stability and reactivity of the molecule, especially the concept of entropy, which reveals that all chemical reactions direct the direction towards disorder. Therefore, it determines how tightly a compound binds to its target.

Table 9
Thermodynamic properties at different temperatures in the range 100-500 Kelvin of the diaqua-bis(indazole-κN^2)bis(nitrato-κO)zinc(II) complex.

T (K)	$C^0_{p,m}$ (J mol^{-1} K^{-1})	S^0_m (J mol^{-1} K^{-1})	ΔH^0_m (kJ mol^{-1})	ΔG_{corr} (kJ mol^{-1})	ϵ_{ZPE} (kJ mol^{-1})
100	159.89	419.20	2.21	802.96	834.75
200	268.07	568.95	7.72	753.34	834.75
300	379.20	702.10	15.65	689.76	834.75
400	480.80	827.86	26.15	613.25	834.75
500	564.69	946.36	38.87	524.54	834.75

$C^0_{p,m}$: Heat capacity, S^0_m: Entropy, ΔH^0_m: Entalphy changes, G_{corr}:Gibbs free energy, ϵ_{ZPE}: Zero point energy

3.12. Thermal analysis

Thermal analysis yields insights into phase transitions, the presence of water during crystallization, and various phases of decomposition [84]. The TGA curve measured in the 20-800°C range for complex exhibits several weight loss phases that cannot be attributed to any simple decomposition process involving simply the initial component. The Zn (II) complex decomposes into five steps, as seen in the TGA thermogram of the title complex in supplementary Fig. S7. The first and second steps occur with an experimental mass loss of 5.3% and 5% in the temperature range from 50°C to 150°C. The thermal event in this step is the result of nitrate anion decomposition. The third step occurs in the temperature interval from 160°C to 200°C, with a mass loss of 19% corresponding to the decomposition of O-H groups. The fourth step takes place between 350℃ and 400℃ which loses a mass of 23.3%, which is defined by the removal of ligand molecules. In the last step, the remainder of the complex was decomposed, which represents 41.3% of the mass.

4. Conclusion

In the present study, the Zn(II) complex of the indazol molecule was

synthesized and then characterized by XRD, UV-Vis, and FT-IR UV-Vis spectroscopy techniques. As a result of X-ray structure analysis, it was determined that the bis(indazole-κN^2)bis(nitrato-κO)zinc(II) complex was formed by two indazole ligands, two nitrate anions, two water molecules, and the Zn(II) metal at the center. Structural investigation reveals an octahedral geometry around the Zn(II) atom. Quantum chemical calculations by using the DFT method confirmed the experimental results and showed good agreement between the experimental and theoretical results in terms of molecular geometry. The DFT, AIM, and Hirsfeld surface analyses are used to investigate the presence of metal-ligand interactions. The predominant interactions in the crystal were identified using the AIM analysis and the NCI-RDG isosurface. By creating ELF and LOL maps, the regions with localized and delocalized electrons were determined for the synthesized structure. We can see that these maps indicate a high degree of electron localization due to covalent bonds around the hydrogen atom. The MEP map shows that the negative potential sites are located at the oxygen atoms of the nitrate group, while the positive potential sites are located at the N1 and N1′ atoms in the pyrazole ring. Hirshfeld surface analysis reveals the possibility of weak and longer intermolecular interactions in the crystalline state. Also, this analysis method showed that H…H(30.9%), C…H (16.2%), and O…H(36.7%) dominate their interactions in the overall crystal packing.

CRediT authorship contribution statement

Ceyhun Kucuk: Writing – review & editing, Writing – original draft, Software, Methodology, Formal analysis, Data curation, Conceptualization. **Sibel Celik:** Writing – review & editing, Writing – original draft, Software, Methodology, Formal analysis, Data curation. **Senay Yurdakul:** Writing – review & editing, Writing – original draft, Supervision, Methodology, Investigation. **Namık Özdemir:** Writing – original draft, Software, Data curation. **Hakan Bülbül:** Writing – original draft, Visualization, Data curation.

Declaration of competing interest

The authors declare that they have no known competing financial interests or personal relationships that could have appeared to influence the work reported in this paper.

Data availability

CCDC 2286961 contains the supplementary crystallographic data for the compound reported in this article. These data can be obtained free of charge from The Cambridge Crystallographic Data Centre via www.ccdc.cam.ac.uk/structures.

Supplementary materials

Supplementary material associated with this article can be found, in the online version, at doi:10.1016/j.molstruc.2024.137666.

References

[1] D.D. Gaikwad, A.D. Chapolikar, C.G. Devkate, K.D. Warad, A.P. Tayade, R. P. Pawar, A.J. Domp, Synthesis of indazole motifs and their medicinal importance: An overview, Eur. J. Med. Chem. 90 (2015) 707–731.

[2] P. Dilipkumar, S. Pooja, Importance of indazole against neurological disorders, Curr. Top. Med. Chem. 22 (14) (2022) 1136–1151.

[3] A.D. Mills, M.Z. Nazer, M.J. Haddadin, M.J. Kurth, N,N-bond-forming heterocyclization: Synthesis of 3-alkoxy-2H-indazoles, J. Org. Chem. 71 (7) (2006) 2687–2689.

[4] T. Zhang, W. Bao, Synthesis of 1 H-indazoles and 1H-pyrazoles via FeBr3/O 2 mediated intramolecular C-H amination, J. Org. Chem. 78 (2013) 1317–1322.

[5] S.G. Zhang, C.G. Liang, W.H. Zhang, Recent Advances in Indazole-containing derivatives: synthesis and biological perspectives, Molecules 23 (11) (2018) 2783.

[6] A.E. Filkale, M.K. Gangwar, I.K. Pandey, R.J. Butcher, Biphenol-based tetradentate N2O2 donor scaffold binuclear Zn(II) and trinuclear Cu(II) Complexes: Synthesis, structure, characterizations, and catalytic cyanosilylation of aldehydes at room temperature, Inorg. Chim. Acta 559 (2024) 121801.

[7] Q. Poladian, O. Şahin, T. Karakurt, B.İ. Ceylan, Y. Kurt, A new zinc(II) complex with N2O2-tetradentate Schiff-base derived from pyridoxal-S-methylthiosemicarbazone: synthesis, characterization, crystal structure, DFT, molecular docking and antioxidant activity studies, Polyhedron 201 (2021) 115164.

[8] S.K. Nandanwar, H.J. Kim, Anticancer and antibacterial activity of transition metal Complexes, ChemistrySelect 4 (2019) 1706–1721.

[9] Z.H. Abd El-Wahab, M.R. El-Sarrag, Derivatives of phosphate Schiff base transition metal complexes: synthesis, studies and biological activity, Spectrochim. Acta A 60 (1-2) (2004) 271–277.

[10] C. Kucuk, S. Celik, S. Yurdakul, E. Coteli, B. Erdem, Synthesis, characterization, thermal, DFT study, antioxidant and antimicrobial in vitro investigations of indazole and its Ag(I) complex, Polyhedron 241 (2023) 116469.

[11] T.R. Fomuta, G. Djimassingar, J. Ngoune, N.O. Ngnabeuye, J.J. Anguile, J. Nenwa, Synthesis, structural characterization and DFT studies of silver(I) complex salt of bis(4,5-dihydro-1H-benzo[g]indazole), Cryst. Struct. Theory. Appl. 6 (2017) 11–24.

[12] T.U. da Silva, E.T. da Silva, K. de Carvalho Pougy, C.H. da Silva Lima, S. de Paula Machado, Molecular modeling of indazole-3-carboxylic acid and its metal complexes (Zn, Ni, Co, Fe and Mn) as NO synthase inhibitors: DFT calculations, docking studies and molecular dynamics simulations, Inorg. Chem. Commun. 135 (2022) 109120.

[13] K. Schwarz, DFT calculations of solids with LAPW and WIEN2k, J. Solid State Chem. 176 (2) (2003) 319–328.

[14] Y.S. Mary, Y.S. Mary, S. Armaković, S.J. Armaković, R. Yadav, I. Celik, P. Yele, B. Chakraborty, Stability and reactivity study of bio-molecules brucine and colchicine towards electrophile and nucleophile attacks: insight from DFT and MD simulations, J. Mol. Liq. 335 (2021) 116192.

[15] I. Erden, A. Hatipoglu, C. Cebeci, S. Aydogdu, Synthesis of D-π-A type 4,5-diazafluorene ligands and Ru (II) complexes and theoretical approaches for dye-sensitive solar cell applications, J. Mol. Struct. 1201 (2020) 127202.

[16] R. Dennington, T. Keith, J. Millam, GaussView, Version 5, Semichem Inc., Shawnee Mission, KS, USA. (2009).

[17] A.D. Becke, Density-functional thermochemistry III. The role of exact exchanege, J. Chem. Phys. 98 (1993) 5648–5652.

[18] H.B. Howsaui, A.S. Basaleh, M.H. Abdellattif, W.M.I. Hassan, M.A. Hussien, Synthesis, structural investigations, molecular docking, and anticancer activity of some novel Schiff bases and their uranyl complexes, Biomolecules 11 (8) (2021) 1138.

[19] M.J. Frisch, G.W. Trucks, H.B. Schlegel, G.E. Scuseria, M.A. Robb, J.R. Cheeseman, G. Scalmani, V. Barone, B. Mennucci, G.A. Petersson, H. Nakatsuji, M. Caricato, X. Li, H.P. Hratchian, A.F. Izmaylov, J. Bloino, G. Zheng, J.L. Sonnenberg, M. Hada, M. Ehara, K. Toyota, R. Fukuda, J. Hasegawa, M. Ishida, T. Nakajima, Y. Honda, O. Kitao, H. Nakai, T. Vreven, J.A. Montgomery, Jr., J.E. Peralta, F. Ogliaro, M. Bearpark, J.J. Heyd, E. Brothers, K.N. Kudin, V.N. Staroverov, R. Kobayashi, J. Normand, K. Raghavachari, A. Rendell, J.C. Burant, S.S. Iyengar, J. Tomasi, M. Cossi, N. Rega, J.M. Millam, M. Klene, J.E. Knox, J.B. Cross, V. Bakken, C. Adamo, J. Jaramillo, R. Gomperts, R.E. Stratmann, O. Yazyev, A.J. Austin, R. Cammi, C. Pomelli, J.W. Ochterski, R.L. Martin, K. Morokuma, V.G. Zakrzewski, G.A. Voth, P. Salvador, J.J. Dannenberg, S. Dapprich, A.D. Daniels, O. Farkas, J.B. Foresman, J. V. Ortiz, J. Cioslowski, D.J. Fox, Gaussian, Inc., Wallingford CT, (2009).

[20] B. Silvi, A. Savin, Classification of chemical bonds based on topological analysis of electron localization functions, Nature 371 (6499) (1994) 683–686.

[21] T. Lu, F. Chen, Multiwfn: A multifunctional wavefunction analyzer, J. Comput. Chem. 33 (5) (2012) 580–592.

[22] W. Humphrey, A. Dalke, K. Schulten, VMD: visual molecular dynamics, J. Mol. Graph. 14 (1996) 33–38.

[23] E.D. Glendening, C.R. Landis, F. Weinhold, NBO 6.0: Natural bond orbital analysis program, J. Comput. Chem. 34 (2013) 1429–1437.

[24] Stoe & Cie, X-AREA (Version 1.18) and X-RED32 (Version 1.04), Stoe & Cie, Darmstadt, Germany, (2002).

[25] G.M. Sheldrick, SHELXT – Integrated space-group and crystal-structure determination, Acta Crystallogr. Sect. A 71 (1) (2015) 3–8.

[26] G.M. Sheldrick, Crystal structure refinement with SHELXL, Acta Crystallogr. Sect. C 71 (1) (2015) 3–8.

[27] O.V. Dolomanov, L.J. Bourhis, R.J. Gildea, J.A.K. Howard, H. Puschmann, OLEX2: a complete structure solution, refinement and analysis program, J. Appl. Crystallogr. 42 (2) (2009) 339–341.

[28] C. Janiak, S. Temizdemir, S. Dechert, W. Deck, F. Girgsdies, J. Heinze, M.J. Kolm, T.G. Scharmann, O.M. Zipffel, Binary [Hydrotris(indazol-1-yl)borato]metal Complexes, $M(Tp^{4Bo})_2$ [1]with M = Fe, Co, Ni, Cu, and Zn: Electronic Properties and Solvent-Dependent Framework Structures through C-H···π Interactions, Eur. J. Inorg. Chem. 6 (2000) 1229–1241.

[29] M.A. Maldonado-Rogado, E. Viñuelas-Zahínos, F. Luna-Giles, F.J. Barros-García, Synthesis and structural characterization of cobalt(II) and zinc(II) complexes with 2-(indazol-1-yl)-2-thiazoline (TnInA). X-ray characterization of $[CoCl_2(TnInA)_2] \cdot C_2H_6O$ and $[(M)(TnInA)_2(H_2O)_2](NO_3)_2$ (M = Co, Zn), Polyhedron 26 (18) (2007) 5210–5218.

[30] A.A.G. Valdivia, M.P. Mendoza, D.C. Lazarte, J. Cepeda, B. Fernández, M. Souto, M.G. Tejero, J.A. García, G.M. Espallargas, A.R. Diéguez, Interpenetrated luminescent metal–organic frameworks based on 1H-Indazole-5-carboxylic acid, Cryst. Growth Des. 20 (7) (2020) 4550–4560.

[31] L. Götzke, K. Gloe, K.A. Jolliffe, L.F. Lindoy, A. Heine, T. Doert, A. Jäger, K. Gloe, Nickel(II) and zinc(II) complexes of N-substituted di(2-picolyl)amine derivatives: Synthetic and structural studies, Polyhedron 30 (2011) 708–714.

[32] A.N. Chekhlov, 4,7,13,16,21,24-Hexaoxa-1,10-Diazoniabicyclo[8.8.8]-Hexacosane Tetra(nitrato)zinc(II): Synthesis and crystal structure, Russ. J. Coord. Chem. 33 (2) (2007) 90–95.

[33] A. Sy, A.H. Barry, F.B. Amor, A. Driss, M. Gayea, A.S. Sall, Bis(imidazole-κN^3)bis (nitrato-κO)zinc(II), Acta Crystallogr. Sect. E 65 (10) (2009) m1238.

[34] H. Pang, X. Zou, B. Xu, H. Zhang, Crystal structure of aqua-bis(1,5-dimethyl-2-phenyl-4-(((*E*)-4-pyridylmethylene)amino)pyrazolidin-3-one-κ*N*)-(nitrato-κ*O*)-(nitrato-κ2*O*,*O*′)zinc(II), $C_{34}H_{34}N_{10}O_9Zn$, Z. Krist. New. Cryst. St. 234 (1) (2019) 121–123.

[35] J. Bernstein, R.E. Davis, L. Shimoni, N.L. Chang, Patterns in hydrogen bonding: functionality and graph set analysis in crystals, Angew. Chem. Int. Ed. 34 (1995) 1555–1573.

[36] S. Gatfaoui, N. Issaoui, S.A. Brandan, T. Roisnel, H. Marouani, Synthesis and characterization of p-xylylenediaminium bis(nitrate). Effects of the coordination modes of nitrate groups on their structural and vibrational properties, J. Mol. Struct. 1151 (2018) 152–168.

[37] T. Sundius, S.A. Brandan, Structural, harmonic force field and vibrational studies of cholinesterase inhibitor tacrine used for treatment of Alzheimer's disease, Heliyon 9 (2023) e717280.

[38] A.B. Rached, W. Maalej, P. Guionneau, N. Daro, T. Mhiri, H. Feki, Z. Elaoud, Synthesis, crystal structure, and vibrational and dft simulation studies of benzylammonium dihydrogen phosphate, J. Phys. Chem. Solids. 123 (2018) 150–156.

[39] M.H. Jamroz, Vibrational energy distribution analysis (VEDA): scopes and limiations, Specrochim. Acta. A 114 (2004) 220–230.

[40] S.E. Makhloufy, E.M. Majdi, A. Ouasri, S. Chtita, M. Saadi, L.E. Ammari, A. Cherqaoui, S. Belaaouad, Synthesis, crystal structure, IR, Raman-spectroscopy and DFT computation of monostrontium phosphate monohydrate, Sr $(H_2PO_4)_2{\cdot}H_2O$, L. Coord. Chem. 73 (16) (2020) 2328–2346.

[41] N.J. Jasmine, C. Arunagiri, A. Subashini, N. Stanley, P.T. Muthiah, Synthesis, X-ray structure analysis, thermodynamic and electronic properties of 4-acetamido benzaldehyde using vibrational spectroscopy and DFT calculations, J. Mol. Struct. 1130 (2017) 244–250.

[42] Y. Erdogdu, M.T. Güllüoglu, Analysis of vibrational spectra of 2 and 3-methylpiperidine based on density functional theory calculations, Spectrochim. Acta A 74 (2009) 162–167.

[43] N. Sundaraganesan, B.D. Joshua, K. Settu, Vibrational spectra and assignments of 5-amino-2-chlorobenzoic acid by ab initio Hartree–Fock and density functional methods, Spectrochim. Acta A 66 (2007) 381–388.

[44] V. Krishnakumar, S. Dheivamalar, R.J. Xavier, V. Balachandran, Analysis of vibrational spectra of 4-amino-2,6-dichloropyridine and 2-chloro-3,5-dinitropyridine based on density functional theory calculations, Spectrochim. Acta A 65 (2006) 147–154.

[45] R.M. Silverstein, F.X. Webster, D.J. Kiemle, D.L. Bryce, Spectrometric identification of organic compounds, John Wiley & Sons, Singapore, 2014. ISBN: 978-0-470-61637-6.

[46] V. Sathyanarayanmoorthi, R. Karunathan, V. Kannappan, Molecular modeling and spectroscopic studies of benzothiazole, J. Chem. (2013) 258519.

[47] J.J.L. González, F.P. Ureña, J.R.A. Moreno, I. Mata, E. Molins, R.M. Claramunt, C. López, I. Alkorta, J. Elguerod, The chiral structure of 1H-indazoles in the solid state: a crystallographic, vibrational circular dichroism and computational study, New J. Chem. 36 (2012) 749–758.

[48] S.A. Brandán, M.L. Roldán, C. Socolsky, A. Ben Altabef, DFT calculation of the chromyl nitrate, $CrO_2(NO_3)_2$: The molecular force field, Spectrochim. Acta A 69 (3) (2018) 1027–1043.

[49] P. Gorai, S. Banerjee, D. Nag, S.K. Mukhopadhyay, A. Saha, Design and synthesis of a novel fluorescent-colorimetric chemosensor for selective detection of Zn(II) and Cu(II) ions with applications in live cell imaging and molecular logic gate, J. Lumin. 205 (2019) 197–209.

[50] L. Sharipova, F. Mamatova, Ir-Spectroscopic Analysis of the Coordination Compounds of Zinc Nitrate with Benzamide And Urea, Int. Scient, J. Sci. Innov. 2 (2) (2023) 65–69.

[51] A.Chaudhary Mamta, Synthesis, DFT calculation, molecular docking studies and biological evaluation of a novel series of Schiff base tetradentate macrocyclic ligands and their Zn(II) complexes as antimicrobial, anti-inflammatory and anticancer agents, Res. Chem. Intermed. 49 (2023) 4671–4712.

[52] X. Ye, D. Wang, K. Yuan, Y. Dong, Z. Chen, C. Huang, Z. Yu, D. Wu, Synthesis, characterization and antibacterial activity of [Zn(formato)2(4,4′-bipy)] complex, J. Mol. Struct. 1225 (2021) 129094.

[53] S.N. Ostad, A. Abedi, V. Amani, P. Karimi, S. Heydarnezhad, Influence of methyl group position in bipyridine ligand on structure and luminescence of related zinc (II) nitrate complexes, J. Iran. Chem. Soc. 13 (2016) 1417–1427.

[54] M. Pandey, S. Muthu, N.M. Nanje Gowda, Quantum mechanical and spectroscopic (FT-IR, FT-Raman,1H,13C NMR, UV-Vis) studies, NBO, NLO, HOMO, LUMO and Fukui function analysis of 5-Methoxy-1H-benzo[d]imidazole-2(3H)-thione by DFT studies, J. Mol. Struct 1130 (2017) 511–521.

[55] A. Thamarai, R. Vadamalar, M. Raja, S. Muthu, B. Narayana, P. Ramesh, R. R. Muhamed, S. Sevvanthi, S. Aayisha, Molecular structure interpretation, spectroscopic (FT-IR, FT-Raman), electronic solvation (UV–Vis, HOMO-LUMO and NLO) properties and biological evaluation of (2E)-3-(biphenyl-4-yl)-1-(4-bromophenyl)prop-2-en-1-one: Experimental and computational modeling approach, Spectrochim. Acta A 226 (2020) 117609.

[56] M.J. Alam, A.U. Khan, M. Alam, S. Ahmad, Spectroscopic (FTIR, FT-Raman, 1H NMR and UV–Vis) and DFT/TD-DFT studies on cholesteno [4,6-b,c]-2′,5′-dihydro-1′,5′-benzothiazepine, J. Mol. Struct. 1178 (2019) 570–582.

[57] B. Sureshkumar, Y.S. Mary, K.S. Resmi, C.Y. Panicker, S. Armakovic, S. J. Armakovic, B.Narayana Van C. Alsenoy, S. Suma, Spectroscopic analysis of 8-Hydroxyquinoline derivatives and investigation of its reactive properties by DFT and molecular dynamics simulations, J. Mol. Struct. 1156 (2018) 336–347.

[58] S.D. Oladipo, G.F. Tolufashe, C. Mocktar, B. Omondi, Ag(I) symmetrical N, N′ -diarylformamidine dithiocarbamate PPh3 complexes: synthesis, structural characterization, quantum chemical calculations and in vitro biological studies, Inorg. Chim. Acta 520 (2021) 120316.

[59] P.R. Spackman, M.J. Turner, J.J. McKinnon, S.K. Wolff, D.J. Grimwood, D. Jayatilaka, M.A. Spackman, CrystalExplorer: a program for Hirshfeld surface analysis, visualization and quantitative analysis of molecular crystals, J. Appl. Cryst. 54 (3) (2021) 1006–1011.

[60] M.J. Mphahlele, M.M. Maluleka, T.P. Mokoena, Spectroscopic, XRD, Hirshfeld surface and density functional theory (DFT) studies of the non-covalent interactions in 2-hydroxy-3-iodo-5-nitroacetophenone, J. Mol. Struct. 1265 (2022) 133471.

[61] S.K. Seth, Structural elucidation and contribution of intermolecular interactions in *O*-hydroxy acyl aromatics: Insights from X-ray and Hirshfeld surface analysis, J. Mol. Struct. 1064 (2014) 70–75.

[62] R. Arulraj, S. Sivakumar, K. Rajkumar, J.P. Jasinski, M. Kaur, A. Thiruvalluvar, Synthesis, crystal structure, DFT calculations and Hirshfeld surface analysis of 3-Chloro-3-methyl-r(2), c(6)-bis(p-methoxyphenyl) piperidin-4-one, J. Chem. Crystallogr. 50 (2020) 41–51.

[63] E.P. Cuadradoa, K. Ferrer, E. Osorioc, I. Brito, J. Cisterna, M. Gutiérrez, Crystal structure, Hirshfeld surface analysis and DFT studies of N-(4-acetylphenyl) quinoline-3-carboxamide, J. Mol. Struct. 1246 (2021) 131162.

[64] R. Hakiri, I. Ameur, S. Abid, N. Derbel, Synthesis, X-ray structural, Hirshfeld surface analysis, FTIR, MEP and NBO analysis using DFT study of a 4-chlorobenzylammonium nitrate $(C7ClH9N)^+(NO3)$, J. Mol. Struct. 1164 (2018) 486–492.

[65] M.J. Alam, S. Ahmad, Quantum chemical and spectroscopic investigations of 3-methyladenine, Spectrochim. Acta A 128 (2014) 653–664.

[66] S. Celik, M. Alp, S. Yurdakul, A combined experimental and theoretical study on vibrational spectra of 3-pyridyl methyl ketone, Spectrosc. Lett. 53 (4) (2020) 234–248.

[67] F.B. Rizwana, J.C. Prasanaa, S. Muthu, C.S. Abraham, Molecular docking studies, charge transfer excitation and wave function analyses (ESP, ELF, LOL) on valacyclovir: A potential antiviral drug, Comput. Biol. Chem. 78 (2019) 9–17.

[68] B.R. Raajaraman, N.R. Sheela, S. Muthu, Spectroscopic, quantum computational and molecular docking studies on 1-phenylcyclopentane carboxylic acid, Comput. Biol. Chem. 82 (2019) 44–56.

[69] C. Morell, A. Grand, A. Toro-Labbe, New dual descriptor for chemical reactivity, J. Phys. Chem. A 109 (2005) 205e212.

[70] B.Q. Sheeba, M.S.M. Mary, M. Amalanathan, C.B. Job, Structural and vibrational spectral investigation on the identification of Non-Linear Optical properties and wave function analyses (electrostatic potential, electron localisation function, localised orbital locator) of 3-Ethoxy Salicilaldehyde, Mol. Simul. 47 (15) (2021) 1217–1233.

[71] S. Murugavel, V.V. Velan, D. Kannan, M. Bakthadoss, Synthesis, crystal structure analysis, spectral investigations, DFT computations, biological activities and molecular docking of methyl(2E)-2-{[N-(2formlyphenyl)(4-metylbrnzene) sulfonamido]metyl}-3-(4-lurophenyl)prop-2enoate a potential bioactive agent, J. Mol. Struct. 1108 (2016) 150–167.

[72] Z. Demircioğlu, G. Kaştaş, Ç.A. Kaştaş, R. Frank, XRD Spectroscopic, Hirshfeld surface, DFT approach, (chemical activity, ECT, NBO, FFA, NLO, MEP, NPA& MPA) of (E)-4-bromo-2-[(4-bromophenylimino)methyl]-6-ethoxyphenol, J. Mol. Struct. 1191 (2019) 129–137.

[73] F. Zayer, W. Dghais, H. Belgacem, Modeling framework and comparison of memristive devices and associated STDP learning windows for neuromorphic applications, J. Phys. D. Appl. Phys. 52 (2019) 393002.

[74] M. Chaabene, F. Zayer, S. Agren, M. Jabli, H. Ghalla, M. Hassen, V. Baouab, R. B Chaâbane, Use of tetraphenyl (hydroxyl) imidazole for colorimetric detection of iodide: Optical properties, computational characterizations, NBO, QTAIM, and NCI-RDG analyses, Inorg. Chem. Comm. 144 (2022) 109917.

[75] A. Soltanabadi, Z. Fakhri, M.T. Azad, Experimental evidence and computational results in the investigation of thermodynamic properties and molecular structure of hydrogen-bonded cyclohexylamine and ethyl methyl ketone system, J. Chem. Thermodyn. 179 (2023) 106984.

[76] U. Koch, P.L.A. Popelier, Characterization of CHO hydrogen bonds on the basis of the charge density, J. Phys. Chem. 99 (1995) 9747–9754.

[77] K. Rayene, D. Imane, B. Abdelaziz, N. Leila, M. Fatiha, G. Abdelkrim, G. Bouzid, L. Ismahan, H. Brahim, O. Rabah, Molecular modeling study of structures, Hirschfield surface, NBO, AIM, RDG, IGM and 1HNMR of thymoquinone/hydroxypropyl-β-cyclodextrin inclusion complex from QM calculations, J. Molec. Struct 1249 (2022) 131565.

[78] P. Mazumdar, A. Kashyap, D. Choudhury, Investigation of hydrogen bonding in small nucleobases using DFT, AIM, NCI and NBO technique, Comput. Theor. Chem. 1226 (2023) 114188.

[79] A. Boughougal, R. Kadri, M. Kadri, J.B. Tommasino, G. Pilet, A. Messai, D. Luneau, Novel copper (II) and zinc (II) complexes with enrofloxacin and oxolinic acid: synthesis, characterization, Hirshfeld surface and DFT/CAM-B3LYPD3BJ studies: NBO, QTAIM and RDG analysis, J. Mol. Struct. 1282 (2023) 135141.

[80] R. Subramaniyan, R. Ramarajan, A. Ramalingam, S. Sambandam, A. Petersamy, A. R. Guerroudj, A.Chouaih N.Boukabcha, Microwave assisted synthesis, vibrational

spectra, Hirshfeld surface and interaction energy, DFT, topology, in silico ADMET and molecular docking studies of 1,2-bis(4-methoxybenzylidene)hydrazine, J. Mol. Struct. 1278 (2023) 134946.

[81] Y.S. Mary, Y. Shyma Mary, A.S. Rad, R. Yadav, I. Celik, S. Sarala, Theoretical investigation on the reactive and interaction properties of sorafenib – DFT, AIM, spectroscopic and Hirshfeld analysis, docking and dynamics simulation, J. Mol. Liq. 330 (2021) 115652.

[82] S.S. Khemalapure, V.S. Katti, C.S. Hiremath, S.M. Hiremath, M. Basanagouda, S. B. Radder, Spectroscopic (FT-IR, FT-Raman, NMR and UV-Vis), ELF, LOL, NBO, and Fukui function investigations on (5-bromo-benzofuran-3-yl)-acetic acid hydrazide (5BBAH): Experimental and theoretical approach, J. Mol. Struct 1196 (2019) 280–290.

[83] S. Janani, H. Rajagopal, S. Muthu, S. Aayisha, M. Raja, Molecular structure, spectroscopic (FT-IR, FT-Raman, NMR), HOMO-LUMO, chemical reactivity, AIM, ELF, LOL and molecular docking studies on 1-Benzyl-4-(N-Boc-amino)piperidine, J. Mol. Struct 1230 (2021) 129657.

[84] N. Dawar, J. Devi, B. Kumar, A. Dubey, Synthesis, characterization, pharmacological screening, molecular docking, DFT, MESP, ADMET studies of transition metal(II) chelates of bidentate Schiff base ligand, Inorg. Chem. Comm. 151 (2023) 110567.